Hydrogen Storage Capacity of Catalytically Grown Carbon Nanofibers

Matthias Rzepka,*,† Erich Bauer,† Gudrun Reichenauer,‡ Thomas Schliermann,§ Babette Bernhardt,|| Klaus Bohmhammel,|| Eva Henneberg,|| Uta Knoll,⊥ Heinz-Eberhard Maneck,⊥ and Wolfgang Braue#

Bavarian Center for Applied Energy Research (ZAE Bayern e.V.), Div. 1, 85748 Garching, Germany, Bavarian Center for Applied Energy Research (ZAE Bayern e.V.), Div. 2, 97074 Würzburg, Germany, Physics Department, Würzburg University, Am Hubland, 97074 Würzburg, Germany, Technische Universität Bergakademie Freiberg, 09599 Freiberg, Germany, Federal Institute for Materials Research and Testing, 12200 Berlin, Germany, and Deutsches Zentrum für Luft und Raumfahrt (DLR), Materials Research Institute, 51147 Köln, Germany

Received: March 16, 2005; In Final Form: June 8, 2005

In 1996, R. T. K. Baker, and N. M. Rodriguez claimed to have synthesized a new type of carbon nanofiber material capable of storing large amounts of hydrogen at room temperature and pressures above 100 bar, thus making it a powerful candidate for a very efficient energy storage system in mobile applications. Consequently, many scientists all over the world tried to test and verify these findings, however, with partly inconsistent results. We present here for the first time independent hydrogen storage measurements for several types of nanofibers, both synthesized by our group following precisely the specifications given in the literature as well as original samples supplied by Rodriguez and Baker for this study. The hydrogen storage capacities at room temperature and pressures up to 140 bar were quantified independently by gravimetric and volumetric methods, respectively. No significant hydrogen storage capacity has been detected for all carbon nanofibers investigated.

1. Introduction

Fuel cells, which convert hydrogen directly and with high efficiency to electric energy, may be one of the main energy converters of the near future. However, the lack of suitable hydrogen storage systems greatly hinders the introduction of fuel cell systems, especially in mobile applications. Commonly used hydrogen storage systems such as pressurized gas tanks, cryo tanks, or metal hydride storage systems all suffer from major drawbacks such as insufficient storage densities, high costs, or short lifetimes.

It was therefore of worldwide interest when, in December 1996, Rodriguez and Baker claimed that their carbon nanofibers can store up to 70 wt % of hydrogen[1−3] at room temperature and 140 bar hydrogen pressure. Table 1 summarizes their published values for different nanofiber samples.

Carbon nanofibers have been known for a long time.[4−7] Their lengths and diameters are typically in the range of 1−100 μm and 10−200 nm, respectively. They can be grown in different morphologies (see, e.g., Table 1) depending on the synthesis parameters applied; details on the effect of the synthesis parameters on the structural properties are given elsewhere.[8−10] The unique microstructure of platelet and herringbone-type nanofibers—consisting of graphene sheets stacked in an angle with respect to the fiber axis—makes them interesting candidates for a variety of applications, for example, gas storage systems,[11] electrochemical devices,[12,13] or catalyst supports.[14]

TABLE 1: Hydrogen Storage Capacities of Carbon Nanofibers Exhibiting Different Fiber Architectures As Published by Rodriguez and Baker[2]

nanofiber structure	adsorbed H_2 in wt %[a]	nanofiber structure	adsorbed H_2 in wt %[a]
tubular	11	herringbone	61
herringbone	58	platelet	54
herringbone	68	platelet	46

[a] The value of adsorbed H_2 is given in units of weight fraction wt(H_2)/wt(H_2 + C).

Rodriguez and Baker concluded from their data that some sort of intercalation of hydrogen atoms or molecules in the carbon nanofibers might provide storage densities highly exceeding the storage density expected for physical adsorption on the fiber surface. To date, the potential mechanism for high-capacity hydrogen storage in carbon nanofibers still remains unclear, but it obviously has to differ from the storage mechanism in activated carbon or carbon nanotubes, where the hydrogen molecules are physically adsorbed at the surface of the micropores (<2 nm) at the inner tube walls or stored in the interstices between adjacent nanotubes, respectively.

In recent years, different groups tried to reproduce the results of Rodriguez and Baker in similar or modified carbon nanostructures. It was claimed[15] that alkali-doped carbon nanotubes can store up to 20 wt % of hydrogen, which later was demonstrated[16] to be only an effect of hydroxide formation as a result of the moisture content in the hydrogen gas applied in the storage tests. In 1999, Fan et al. and Cheng et al.[17,18]

* Corresponding author. Tel: +49-89-32944231. E-mail: Rzepka@muc.zae-bayern.de.
† Bavarian Center for Applied Energy Research, Div. 1.
‡ Bavarian Center for Applied Energy Research, Div. 2.
§ Würzburg University.
|| Technische Universität Bergakademie Freiberg.
⊥ Federal Institute for Materials Research and Testing.
Materials Research Institute.

10.1021/jp051371a CCC: $30.25
Published on Web 07/14/2005

TABLE 2: Carbon Nanofibers Investigated in the Framework of This Study

	supplier	catalyst	catalyst pretreatment sequence gas composition (gas flow of components (Nml/min)), t_{pre} (min), T_{pre} (°C)	synthesis parameters gas composition (gas flow of components (Nml/min)), t_{CVD} (min), T_{CVD} (°C), amount of catalyst applied (mg)
#1	Catalytic Materials Inc. F1-21	n.sp.[a]	n.sp.	n.sp.
#2	Catalytic Materials Inc. F1-27	n.sp.	n.sp.	n.sp.
#3	Catalytic Materials Inc. F1-28	n.sp.	n.sp.	n.sp.
#4	Catalytic Materials Inc. F1-63	n.sp.	n.sp.	n.sp.
#5	Catalytic Materials Inc. F1-64	n.sp.	n.sp.	n.sp.
#6	Catalytic Materials Inc. G1	n.sp.	n.sp.	n.sp.
#7	BAM, Berlin, synthesized according to ref 9	$Fe_{0.7}Cu_{0.3}$	He, 60 min, 25...500 °C H_2/He (10/90), 120 min, 500 °C	C_2H_4/H_2/He (10/60/30) 120 min, 600 °C, 50 mg
#8	BAM, Berlin, synthesized according to refs 19 and 20	$Ni_{0.98}Cu_{0.02}$	He, 60 min, 25...350 °C H_2/He (10/90), 120 min, 350 °C	C_2H_4/H_2 (20/5) 120 min, 600 °C, 120 mg
#9	BAM, Berlin, synthesized according to ref 21	$Fe_{0.85}Ni_{0.1}Cu_{0.05}$	He, 60 min, 25...500 °C H_2/He (10/90), 120 min, 500 °C	C_2H_4/H_2/He (10/60/30) 120 min, 600 °C, 50 mg
#10	ZAE Bayern, Würzburg	$Ni_{0.7}Cu_{0.3}$	H_2/He (9/91), 60 min, 25...600 °C H_2/He (9/91), 60 min, 600 °C He; 60 min, 600 °C;	C_2H_4/H_2 (48/12) 90 min, 600 °C, 50 mg
#11	ZAE Bayern, Würzburg	$Ni_{0.7}Cu_{0.3}$	H_2/He (9/91), 120 min, 600 °C	C_2H_4/H_2 (80/20) 60 min, 600 °C, 12 mg

[a] Not specified by supplier.

reported on up to 13 wt % hydrogen storage capacity for tubular-shaped vapor-grown carbon nanofibers, whereas in graphitic nanofibers Gupta and Srivastava measured up to 10 wt % hydrogen;[19,20] this range was confirmed by Browning et al.[21] which found a hydrogen storage capacity of 7 wt % for carbon nanofibers.

Besides these optimistic publications, many other experimental results showed no hydrogen storage capacity at all in carbon nanofibers. Measurement of the hydrogen uptake with a microbalance performed for vapor-grown nanofibers by Ströbel et al. yielded values below 1.5 wt %;[22] this tendency was confirmed by Ahn et al.[23] who measured values below 1 wt %. In the last few years, similar results have been published for several nanostructures.[24−26]

Therefore, the issue of the hydrogen storage potential and mechanism of carbon nanofibers is still unresolved. One possible explanation for the great discrepancies between the published values could be a strong dependence of the storage capacity on details of the carbon fiber synthesis and the activation process prior to the storage experiment. Therefore, no final statement in terms of the hydrogen uptake of a certain type of fiber can be made when the carbon nanofibers investigated have been synthesized by different groups. For a conclusive storage test, identical nanofiber batches from the same source have to be employed.

For the study presented, we therefore investigated samples provided by Rodriguez and Baker. In addition, we also synthesized carbon nanofibers according to the specifications given by Baker and Rodriguez,[8,27] Gupta et al.,[19,20] and Browning et al.[21] Special care has to be taken when measuring the hydrogen uptake especially if only a small amount of sample material (<100 mg) is available. For a detailed discussion of the experimental difficulties and possible sources of experimental errors, see, for example, refs 3, 28, and 29. To obtain the most reliable results, we measured the hydrogen uptake with three different experimental methods including volumetric adsorption, volumetric desorption, and a gravimetric technique.

2. Materials

As published by Rodriguez and Baker et al.,[2,3] some batches of their carbon nanofibers showed hydrogen uptake capacities in the range between 10 and 70 wt %. In the meantime, they have established a standardized synthesis procedure yielding a reproducible fiber composition and morphology. The hydrogen storage capacity of these fibers, however, is lower, but it is still in the range between 2 and 4 wt %[30] depending on the pretreatment (activation) procedure prior to hydrogen loading applied. For an independent test of the hydrogen storage capacity of these fibers, we have examined a total of six batches of catalytically grown carbon nanofibers provided by Rodriguez and Baker (Table 2).

In addition to these external samples, we also synthesized carbon nanofibers in our laboratories using catalysts following the specifications published for the materials with high hydrogen storage capacity by Rodriguez and Baker,[9,31] Gupta and Srivastava,[19,20] and Browning et al.,[21] respectively (see also Table 2). The fibers were synthesized according to these procedures with various catalysts and by applying ethylene/hydrogen gas mixtures. The metal powder catalysts used were precipitated from their nitrate solutions as carbonates, calcinated in air at 400 °C for 4 h, and subsequently reduced with 10% H_2 in He at the temperatures given in the respective references (Table 2). The synthesis of the carbon nanofibers was carried out in horizontal quartz tube furnaces of different sizes (furnace at ZAE Bayern, Würzburg: inner diameter 45 mm, length 100 cm; furnace at BAM, Berlin: inner diameter 38 mm, length 40 cm) at 600 °C with an ethylene/hydrogen ratio of 4:1 (samples #8, #10, and #11) and 1:6 (samples #7 and #9), respectively.

3. Characterization Techniques

Complementary to the measurements of the hydrogen storage capacity, all CNF (carbon nanofiber) specimens have been fully characterized in terms of structural, morphological, and chemical properties.

3.1. Structure and Morphology. *Scanning Electron Microscopy (SEM)/Transmission Electron Microscopy (TEM).* The morphological characterization of the CNF was performed with a Hitachi 4100 SEM.

A Philips Tecnai F 30 transmission electron microscope operating at an acceleration voltage of 300 kV has been employed for the TEM investigations. The structural variants of the carbon phase and the metallic particles retained from the catalyst have been characterized via the combination of high-resolution phase contrast imaging (HREM), selected and convergent electron diffraction (SAD, CBED), X-ray microanalysis (EDS), and z-contrast imaging with a high-angle-annular-dark-field (HAADF) detector in STEM mode. TEM specimens were prepared via ultrasonic dispersion of as-received CNF in isobutyl alcohol followed by the deposition of a drop of the suspension on a holey carbon-film Pt-support grid. No supplementary thinning technique was applied.

N_2-Sorption. The nitrogen sorption measurements were carried out using a commercial sorption apparatus (ASAP 2000 with micropore option, Micromeritics, GA) equipped with 100, 10, and 1 mbar pressure transducers.

The samples were degassed at 350 °C in a vacuum for several hours until a stable gas pressure was reached; the nanofibers were stepwise exposed to an increasing nitrogen pressure at 77.4 K covering the relative pressure range from 0.001 to 1. Typically, 100 mg of carbon material was used for each analysis. The nitrogen sorption isotherms were evaluated to determine the BET surface area in the relative pressure range between 0.04 and 0.24 using standard BET theory.[32] The micropore volume was determined from a Dubinin−Radushkevich (DR) analysis of the sorption data in the relative pressure range of 0.001−0.1.[32]

XRD. X-ray diffraction (XRD) was carried out with a Philips PW 1140 diffractometer in reflection geometry using Cu Kα radiation employing ground CNF material. The structural carbon variant in CNFs were characterized by the interplanar spacing d_{002} of the graphite (002) reflection.[33]

Raman Spectroscopy. The Raman spectra of the nanofibers were taken with a micro-Raman setup (LabRam, Jobin-Yvon-Horiba). The spectrometer has a focal length of 300 nm and is equipped with a 1800-lines/mm grating. The spectral solution was about 5.70 cm^{-1}. The 514.532 nm line of an argon laser with a power of about 80 mW was used as the excitation wavelength. The scattered light was detected by a CCD camera operating at 220 K. An Olympus Mplan 10 objective focused the laser light onto the samples. To prevent the samples from being modified, damaged, or heated, the intensity of the laser light was reduced with filters.

Typically, the Raman intensity was collected from 800 to 1900 cm^{-1} covering the wavenumber regime of the characteristic first-order Raman bands of graphitic carbons, the disorder induced D-band (at approximately 1350 cm^{-1}) and the G-band (at approximately 1580 cm^{-1}). The Raman spectra can be evaluated in terms of width, position, and relative integrated intensities of the first-order Raman bands to extract trends in terms of the crystallinity[34] of the carbon nanofibers.

X-ray Photon Emission Spectroscopy (XPS). The total amount of oxygen present at the fibers surface as well as the chemical environment of oxygen and carbon was investigated by XPS using an ESCALAB 200X (VG Instruments, East Grinstead, U.K.). For the experiment, ground CNF material was attached to one side of a double-sided adhesive Scotch tape, and the second side of the tape was glued to the sample holder. The sample was exposed to Mg Kα radiation (1253.6 eV). For data evaluation, the software ECLIPSE provided with the instrument was applied. For the analysis of the C 1s peak, the program UNIFIT (version 32-33, 2001, University Leipzig) was used.

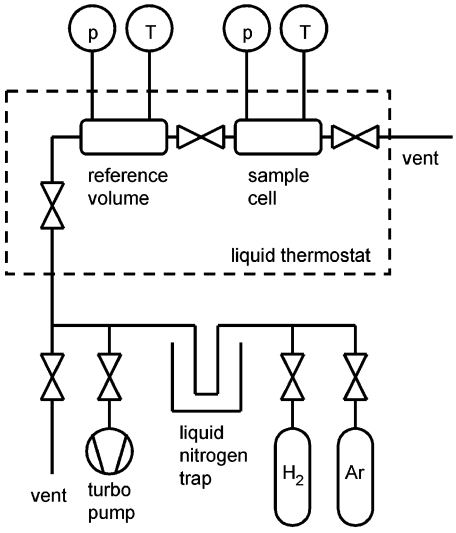

Figure 1. Schematic setup of the volumetric apparatus. The reference volume and the volume of the sample cell are about 13 and 8 mL, respectively.

TDS. For further investigation of the active surface groups, thermodesorption spectra have been collected with a custom-built quadrupole mass spectrometer (Prisma, Pfeiffer Vacuum). In the temperature range from −100 to +900 °C, the desorbing gases are analyzed and recorded. In a typical experiment, 10 mg of the fibers were heated from room temperature to 900 °C with a rate of 10 K/min while monitoring the characteristic masses of released surface groups. This equipment was also used to activate samples of about 200 mg for hydrogen uptake experiments.

3.2. Hydrogen Storage. Special care has to be taken to avoid artifacts during measuring hydrogen uptake from small amounts (<100 mg) of carbon nanofiber samples. To achieve maximum reliability, we have performed three independent measurements with different equipment for each of the samples. In the following sections, experimental setups are described in detail.

Volumetric Apparatus. The experimental setup for the volumetric measurements is shown schematically in Figure 1. The central section of the apparatus consists of two high-pressure cells interconnected by a valve. This section of the instrument is thermally stabilized by a thermostat to ±0.01 °C to avoid thermal drifts which otherwise would dominate the experimental error. In addition, the actual temperature inside each cell is measured independently via thermocouples. The gas pressure is measured by two piezoresistive pressure transducers (resolution 0.01 bar) connected to the central cells by thin, stainless-steel capillaries. A difference between room temperature and thermostat temperature is accounted for by corrections for the amount of gas inside these capillaries. All temperature and pressure sensor values are recorded automatically by a PC. To remove residual water in the hydrogen (6.0 grade) used for the storage analysis, a liquid nitrogen trap was inserted in the gas supply line. High-pressure tests over several days showed no detectable leakage rate for the two central cells (leak rate <0.01 bar/day).

Prior to each measurement, the sample was weighed and inserted into the sample cell. Inside the sample cell, the carbon fibers are enclosed in a gas-permeable microfilter element to avoid the spreading of the fibers inside the apparatus especially upon fast pressure changes. Then—as described later—optional

TABLE 3: Summary of the Characterization Results for the Pristine Samples

fiber	morphology	density (g/cm^3)[a]	BET surface (m^2/g)[b]	micropore volume (cm^3/g)	surface oxygen (at.-%)[c]	d_{002} (nm)[d]
1	herringbone	1.98	119		7	0.343
2	herringbone	2.03	53		8	0.341
3	herringbone	1.99	31		6	0.342
4	herringbone	2.00	271	0.106	1	0.343
5			263	0.096		
6	herringbone	2.14	150	0.061	3	0.339
7	herringbone	2.17	94	0.038	1.7	0.337
8	segmented	2.05	175	0.065		0.341
9	herringbone	2.13	116	0.051		
10	herringbone		200	0.080		0.346
11	herringbone		144	0.051		0.347

[a] The densities were determined via He pycnometry. [b] BET surface areas and micropore volumes were measured with nitrogen sorption. [c] XPS measurements provided the surface oxygen content. [d] The d_{002} values were derived from XRD measurements.

activation procedures can be applied. Subsequently, the whole apparatus is evacuated for several hours by a turbo molecular pump to a pressure level below 10^{-7} mbar. Finally, the valve connecting the two high-pressure cells is closed.

The hydrogen uptake of the sample at about 50, 90, and 140 bar was measured in a three-stage process. At the beginning of each stage, the reference volume is filled with hydrogen to a certain pressure level (90, 140, and 200 bar, respectively). After about 30 min, the whole system is in thermal equilibrium, and the valve to the sample cell is opened. Due to the expansion of the hydrogen gas into the sample cell volume, the pressure in the sample cell increases while the pressure in the reference volume decreases to a final value of about 50, 90, and 140 bar (values determined by the volumes of the reference and the sample cell). An uptake of hydrogen by the sample will cause an additional pressure decrease. If the time constant for the hydrogen absorption is high (e.g., several hours), then the corresponding pressure drop can be recorded directly as the difference between the gas pressure immediately after opening the valve and the final pressure after several hours. However, if the time constant is short (e.g., milliseconds), the additional pressure drop has to be calculated. To achieve sufficient accuracy we have applied the van der Waals equation

$$(p + an^2/V^2)(V - bn) = nRT \qquad (1)$$

with p and T the actual pressure and temperature of the hydrogen gas, $R = 8.314$ J/(mol K), the gas constant, a and b the (gas specific) van der Waals constants, and n the amount of hydrogen gas (in moles). V is the volume of the sample cell, the reference volume, or—if the valve is open—the combined volume of both cells. For each experiment, the volume of the sample cell is corrected for the displaced volume of the carbon sample assuming a bulk density of the sample of 2.1 g/cm^3 (see Table 3). Following eq 1, the amount n_1 of gas before opening the valve is calculated with the appropriate pressure and temperature p_1 and T_1. Similarily, the amount n_2 after opening the valve is calculated with p_2 and T_2. The difference $n_1 - n_2$ directly yields the amount of gas adsorbed.

The values a and b can be taken from the literature, and the volumes V can be determined experimentally. However, to achieve the highest accuracy possible and to avoid any additional systematic errors, we determined all values experimentally in runs without any sample or with steel reference samples with well-defined volumes. As in these runs no gas should be adsorbed, the values a, b, and V_i can be determined by fitting them to the experimental data. This procedure leads to an experimental error of about 0.04 mg (Figure 2).

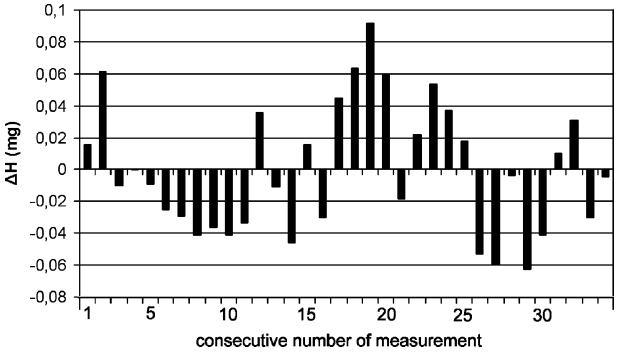

Figure 2. Calibration experiments data (without carbon samples). The apparent hydrogen uptake reflects the experimental inaccuracy of the volumetric instrument of approximately ±0.04 mg.

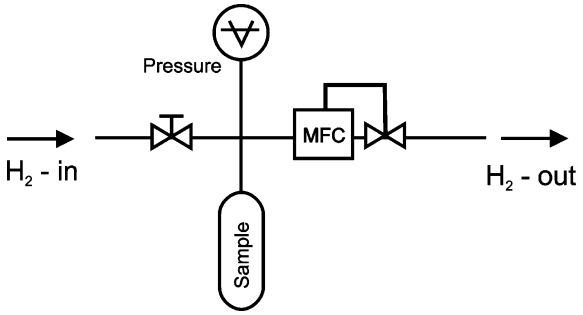

Figure 3. Schematic diagram of the volumetric desorption setup.

Desorption Measurement. The apparatus shown in Figure 3 was designed for measuring hydrogen desorption from a storage material. In a typical experiment, 200−250 mg of the material was loaded in the heatable steel vessel (total volume 46.7 cm^3). After evacuation at 10^{-7} mbar, hydrogen at room temperature was dosed onto the sample in steps of 30−40 bar until a pressure of 130 bar was reached. For the experiments, hydrogen with a purity of 99.999% (5.0) was used; possible traces of water were removed by a liquid nitrogen cold-trap. Twenty-four hours was allowed for the hydrogen uptake and the equilibration of the system.

The amount of hydrogen in the vessel was then calculated from the pressure, the temperature, and the volume of the apparatus (reduced by the sample volume). For this calculation, the van der Waals equation was used. Then the hydrogen pressure was slowly released to atmospheric pressure; the amount of hydrogen released was quantified by the mass flow controller (MFC) in the outlet line (Figure 3). The hydrogen uptake by the material under investigation results in a difference between the initially calculated amount of hydrogen dosed to the vessel and the amount of hydrogen released. This method is 10 times less sensitive as the volumetric method described above, but is very simple; it is also less sensitive to leaks of the apparatus. As confirmed by dry runs, a minimum storage capacity of 3 wt % can be reliably detected.

Gravimetric Apparatus. To confirm the reliability of the volumetric data, we independently determined the hydrogen storage capacity applying a further experimental technique. In the volumetric experiments, the effect of the hydrogen adsorption on the gas pressure in the volume of the sample cell is evaluated to calculate the storage capacity. The third experimental technique records the mass increase of the sample due to hydrogen adsorption with a high-accuracy balance. The principle of the experimental setup is shown in Figure 4.

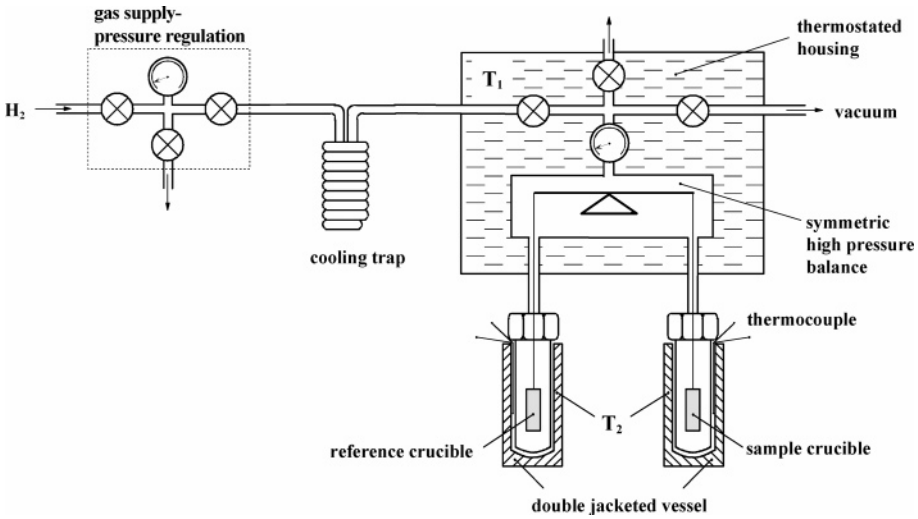

Figure 4. Scheme of the gravimetric apparatus.

We used a modified Sartorius Supermicro S3D-P with balance chambers, which can be pressurized up to 150 bar. While the weighing cell is kept at a constant temperature ($T_1 = 40$ °C), each of the suspended cells can be thermostated at a temperature between −40 and 500 °C. Buoyancy corrections of the sample and the reference have been performed using

$$\Delta m = \frac{\frac{mM_{H_2}}{\rho}p}{RT + \left(b - \frac{a}{RT}\right)p} \qquad (2)$$

with m and ρ the mass and the density of the sample, M_{H_2} the molar mass of hydrogen, R the gas constant, and T and p the temperature and pressure of the hydrogen gas, repectively. As van der Waals constants we used $a = 202\,000$ (cm^6 bar) mol^{-2} and $b = 22.34$ cm^3 mol^{-1}. An additional buoyancy correction for the weighing system was determined by measurements with empty crucibles under otherwise identical conditions. The resulting overall relative error for the determination of the sample mass was about 0.25% at a typical net weight of the sample of 10 mg.

The experimental procedure was as follows: About 5−10 mg of carbon sample was weighed and placed into the sample crucible. The same mass of NaCl (which has a similar density as carbon nanofibers) was placed into the reference crucible. Then the whole balance chamber was rinsed with hydrogen (purity 6.0) for several hours and subsequently evacuated with an oil pump until both pressure and mass were stable. Similar to the volumetric setups, an optional pretreatment procedure can be applied to the sample prior to the actual adsorption experiments. Hydrogen adsorption was measured under isothermal conditions at 25 °C in steps of maximum 40 bar up to a maximum pressure of 140 bar.

Reference Measurements. We measured the hydrogen storage capacity of two reference samples to confirm the accuracy of the volumetric and gravimetric techniques applied. Figure 5 shows the result for an activated carbon sample. Both experiments are in good agreement. The measured adsorption isotherm is also well predicted by the results of Monte Carlo simulations for various shaped pore geometries.[35]

Figure 6 shows the result of the volumetric method for a commercial metal hydride getter. At a final gas pressure of 19.3 bar, the volumetrically measured hydrogen uptake is 0.93 wt %. This is in very good agreement with the value from the data sheet provided by the supplier of the sample.[36]

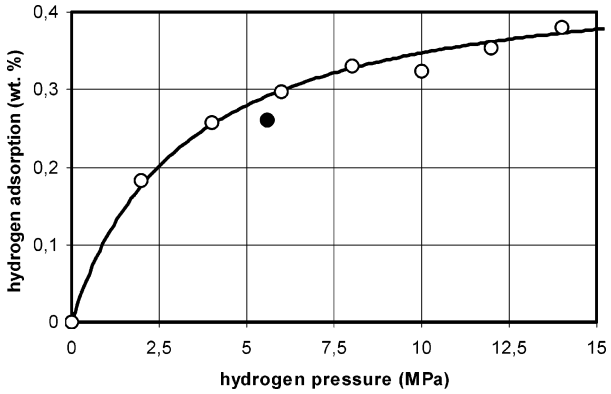

Figure 5. Hydrogen uptake by an activated carbon sample at room temperature (open circles, gravimetric measurement; dot, volumetric measurement).

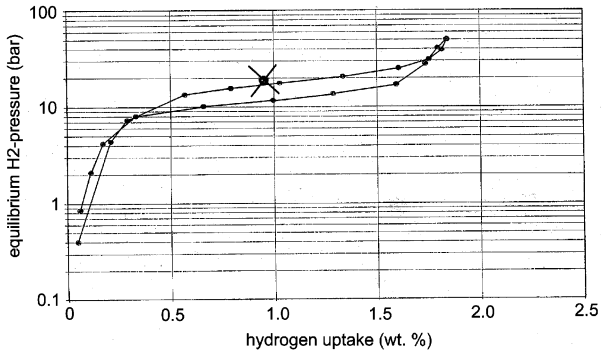

Figure 6. Comparison of the H_2 uptake measured for a commercial metal hydrid at 19.3 bar (cross symbol) with the ad-/desorption isotherms provided by the supplier.[36]

4. Results and Discussion

4.1. Structure and Morphology of the Samples Investigated. A series of six CNF batches (samples #1 through #6, Table 2) has been supplied by Catalytic Materials Inc. SEM images of five batches are compiled in Figure 7. On a micrometer scale, the fibers show the characteristic ribbonlike morphology. The fiber thickness distribution is rather broad containing fibers between 200 and 600 nm in diameter. Coiled fibers may also be present. On the microscopic scale, the

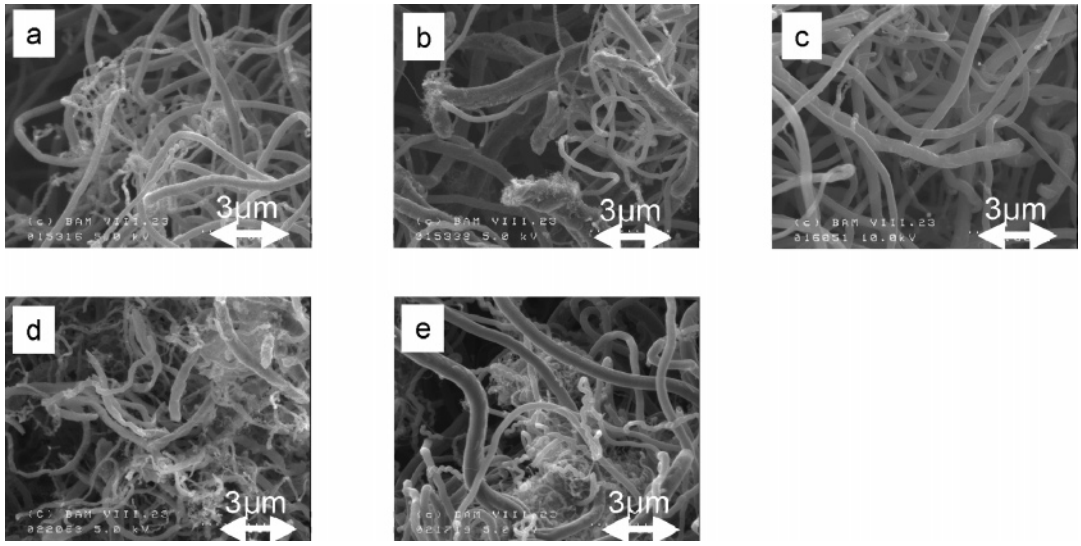

Figure 7. Ribbonlike morphologies (SE images) of different CNF samples supplied by Catalytic Materials Inc.: (a) #1 (F1-21), (b) #2 (F1-27), (c) #3 (F1-28), (d) #4 (F1-63), and (e) #6 (G1).

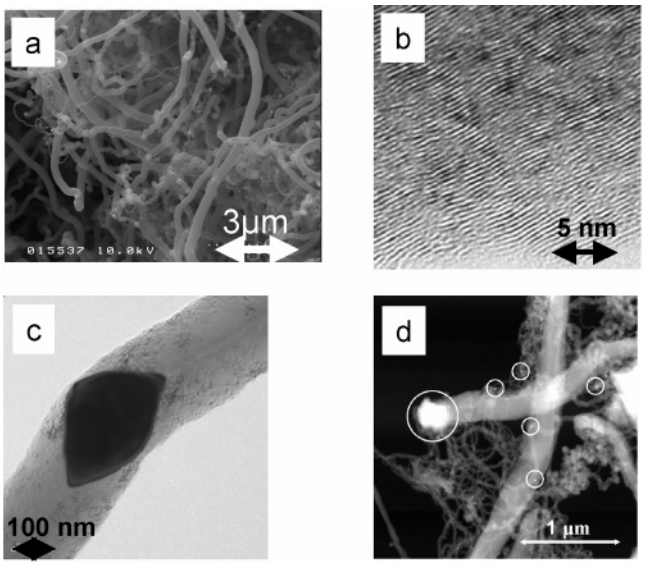

Figure 8. Herringbone-type CNF batch #7 (see Table 2) synthesized on an Fe/Cu catalyst following the processing route by Rodriguez and Baker:[9] (a) SE image showing CNF size distribution within the batch, (b) HREM image of wrinkled (002) basal planes of graphitic carbon, (c) faceted Fe−Cu catalyst particle triggering herringbone-type growth mechanism (TEM, BF), and (d) catalyst distribution within the batch as imaged with a HAADF detector in STEM mode.

herringbone-type arrangement of graphene layers inclined with respect to the fiber growth axis is dominating.

In addition to the samples provided by Rodriguez and Baker, five different CNF batches (samples #7 through #11, Table 2) have been synthesized in the framework of this study and processed following the specifications given in the literature.[8,9,19−21]

A herringbone-type CNF batch (#7, Table 2) employing an Fe/Cu catalyst has been synthesized according to the route given by Rodriguez and Baker in ref 9. The microstructural characteristics of this type of carbon nanofiber are displayed in Figure 8. Notably, the (002) basal planes are wrinkled in the HREM image (Figure 8b) indicating a substantial amount of structural disorder due to heteroatoms present in the graphitic structure. This was confirmed as a general feature for all CNF batches investigated in this study.

Two more batches of nanofibers were synthesized using a Ni/Cu (7/3) powder catalyst (#10 and #11, Table 2) known as one of the most effective catalyst systems for nanofiber synthesis.[8] The SEM images in Figure 9 reveal herringbone-type nanofibers exhibiting a broad diameter distribution (especially batch #11). The sometimes very long fibers of batch #10 (<50 μm, Figure 9) show rather smooth surfaces, whereas in batch #11, considerable amounts of twisted nanofibers together with more irregularly shaped fibers are present (Figure 9).

The CNF batch #8 (Gupta's[19,20] formula) exhibits a segmented fiber architecture (Figure 10) which should be favorable for gas storage applications. As shown in Figure 10b, the graphene layers are stacked indeed parallel to the base of the Ni/Cu particle following a growth mechanism as suggested by Chen et al.[37]

CNFs exhibiting a coiled morphology were obtained with Browning's synthesis parameters[21] employing an Fe/Ni/Cu catalyst (Figure 11).

Supplementary to high-spatial-resolution techniques (SEM, TEM), bulk characterization integral methods such as nitrogen sorption, X-ray diffraction, and Raman spectroscopy were applied to obtain a complete dataset of the samples studied.

In Figure 12, the sorption isotherms of the nanofibers are plotted. Remarkably different nitrogen uptakes are found in the very low relative pressure regime, which is dominated by micropore adsorption, at medium relative pressures (i.e., 0.1−0.4) where multilayer adsorption takes place as well as at relative pressures above 0.4 where capillary condensation in mesopores is predominant. Hence, the quantitative evaluation of the data (Table 3) exhibits a wide scatter of both the BET surface areas (31−271 m^2/g) and the micropore volumes (0.04−0.11 cm^3/g). The latter indicates differences in the microstructural arrangement of the microcrystallites and/or the presence of surface roughness.

Since the BET surface area represents the sum of the specific surface located in the micropores within the fibers and the size of the outer surface of the fibers, differences in this quantity can be attributed to different fiber diameters or diameter distributions within the batches and surface roughness (microporosity) which includes the presence of more exotic nanofiber types. For some samples, a slight hysteresis loop at large relative pressures is present; the course of the sorption curve in this regime is influenced by both the size and shape of mesopores (<50 nm) within or in between the carbon nanofibers. In the latter case, the mechanical characteristics of the loose

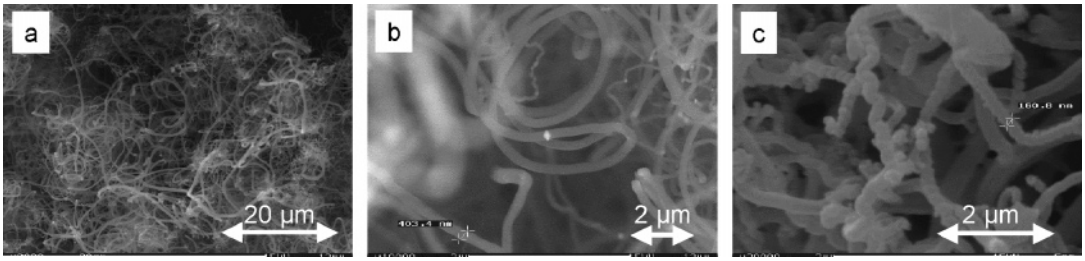

Figure 9. Herringbone-type CNF batch #10 and #11 synthesized using a Ni/Cu (7/3) powder catalyst: (a) very long regular-shaped CNF (#10), (b) fishbone-like CNF exhibiting bidirectional growth characteristic (#10), and (c) regular and irregular CNF, that is, twisted morphologies (#11).

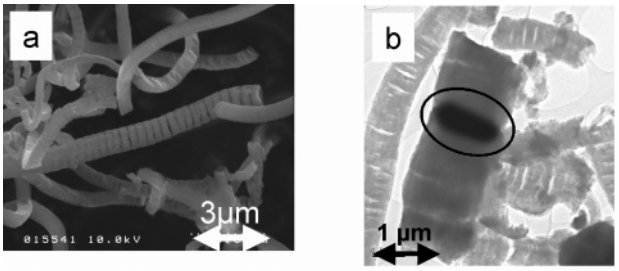

Figure 10. Segmented fiber architecture of batch #8 (see Table 2) following the process route by Gupta et al.:[19,20] (a) coarse-scale fiber microstructure (SE image) and (b) typical location of Ni/Cu catalyst within CNF (TEM bright field), see encircled area.

nanofiber agglomerates can play a crucial role since upon adsorption the capillary tension of the condensing nitrogen is locally compressing the ground sample thus preventing a straightforward interpretation of the data.

For quantification of fiber crystallinity, the interplanar spacing and full width at half maximum (fwhm) of the (002) graphite reflection were derived from X-ray diffraction patterns. The results are summarized in Table 3. For all samples, the interplanar distances are larger than the value for graphite (0.3354 nm); this is consistent with the turbostratic microstructure of the fibers and the presence of heteroatoms as detected by analytical TEM.

All samples show a similar crystallinity except for the samples #6 and especially #7, where the crystallinity is significantly enhanced resulting in smaller d_{002} values accompanied by larger microcrystallite sizes. The behavior of sample #7 is in accordance with earlier findings, namely, that Fe/Cu catalyzed nanofibers exhibit a considerably higher crystallinity than Ni/Cu catalyzed fibers.[9,39]

The latter result is confirmed by Raman measurements. The Raman spectra of all fibers synthesized in our laboratories (except for sample #7) show a similar fingerprint (Figure 13) that is characteristic for Ni/Cu catalyzed nanofibers: Two strong bands at about 1340 cm^{-1} (D-band) and 1600 cm^{-1} (G-band)[34] indicate the existence of a sp^2 carbon arranged in small microcrystallites and maybe some less organized carbon. It is interesting to note that the Raman spectra of the fibers supplied by Catalytic Materials Inc. show almost an identical pattern. In contrast, the half widths of the spectrum for sample #7 are significantly smaller, and the G-band shows a clearly visible shoulder at higher wavenumbers in accordance with a higher crystallinity of the nanofibers.

Activation Procedures. Besides the CNF processing paths, hydrogen storage is largely dependent on the pretreatment of the fiber prior to hydrogen loading. As described in the literature, the activation of the carbon materials is an important step for maximizing the hydrogen storage capacity.[3,21,38] A different or missing pretreatment of the samples may in part explain the strongly varying results found by different groups. Besides removal of surface groups and a general cleaning of the surface, a high-temperature activation may also lead to more distinctive structural changes of the nanofibers. We applied the precise activation procedure given by Rodriguez and Baker[40] to the pristine CNF specimens provided by them to ensure comparability between our results and their data, that is: (a) heating while purging with argon from room temperature to 925 °C in 35 min; (b) holding the temperature at fixed argon flow at 925 °C for 60 min; (c) cooling down to room temperature in about 60 min at continuous argon flow; (d) transferring the sample to the hydrogen storage measurement cell, however, exposing it to atmosphere for less than 10 min; (e) heating the sample under argon flow inside the measurement cell at 200 °C for a minimum of 10 h.

Compared to the characteristics of the pristine fibers, remarkable microstructural changes involving the graphitic fiber architecture, the distribution of catalyst particles, and the surface topology of the fibers take place upon activation in argon atmosphere for all CNF batches investigated. This effect is highlighted for batch #2, sample F1-27 (Figure 14) from Catalytic Materials Inc. and batch #8 (Figure 15), respectively.

Defining the front edge and the truncated cone of the pristine herringbone-type morphology as tip and tail sections (Figure 14a) for the sake of simplicity, Figure 16, illustrates the continuous loss of structural integrity in the fiber tip section due to gaps formed between the graphene layers. It should be noted that the formation of graphite loops at the fiber periphery significantly increases the surface roughness. In addition, high-temperature activitation of CNFs gives rise to a considerable enrichment of catalyst particles at damaged tip or tail sections (Figure 14c) and agglomerates of newly formed, extremely fine-grained, nanotube-type CNF fuzz usually concentrated at tail sections (Figure 14d) or fracture surfaces from individual fibers.

Interestingly, high-temperature activation introduces quite similar microstructural changes to the segmented fibers (batch #8, parts a through c of Figure 15) suggesting that a general damage mechanism is effectively independent of the different CNF characteristics involved.

The formation of graphite loops at the fiber periphery has been attributed to surface reconstruction upon the release of heteroatoms (e.g., hydrogen) from highly active edge sites during heat treatment at CNFs.[41,42] However, with 1800−3000 °C, the temperatures applied in these studies have been considerably higher as compared to the temperature of 925 °C that we used in our activation experiments. This aspect requires further clarification.

The very obvious redistribution of catalyst material upon high-temperature activation of CNFs may be explained by the fact that transition metals easily wet on carbon materials after heat treatment in Ar atmosphere at 1000 °C for several hours if the defect density is sufficiently high.[43] This is certainly the case for CNFs, and it may be anticipated that the well-pronounced

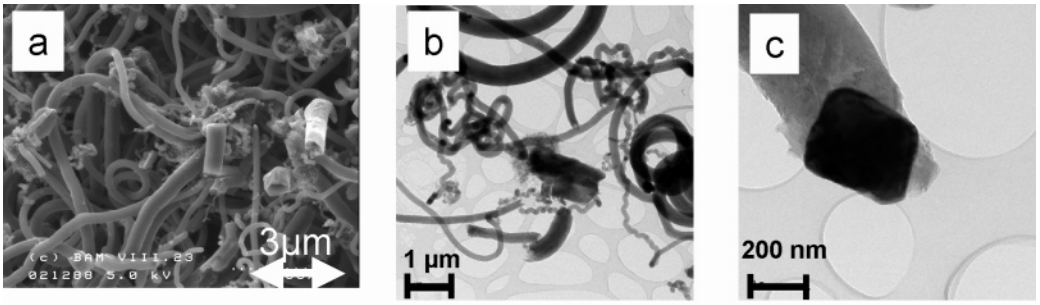

Figure 11. Coiled carbon nanofibers from batch #9 (Table 2) following the processing route by Browning et al.[21] over a Fe/Ni/Cu catalyst: (a and b) coarse-scale CNF microstructure (SE image vs. TEM bright field), (c) faceted catalyst location at the CNF tip.

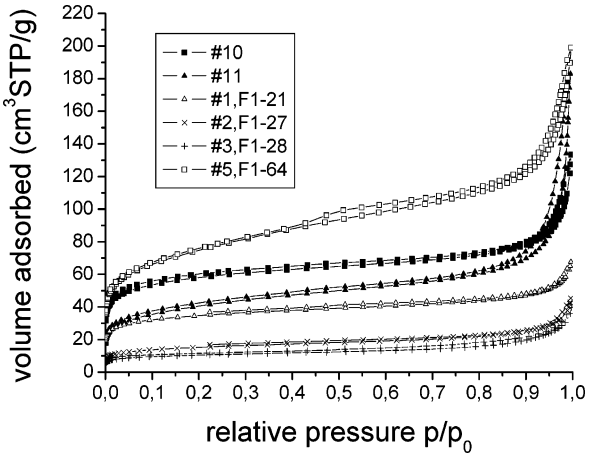

Figure 12. Nitrogen sorption isotherms taken at 77 K for different types of herringbone nanofibers.

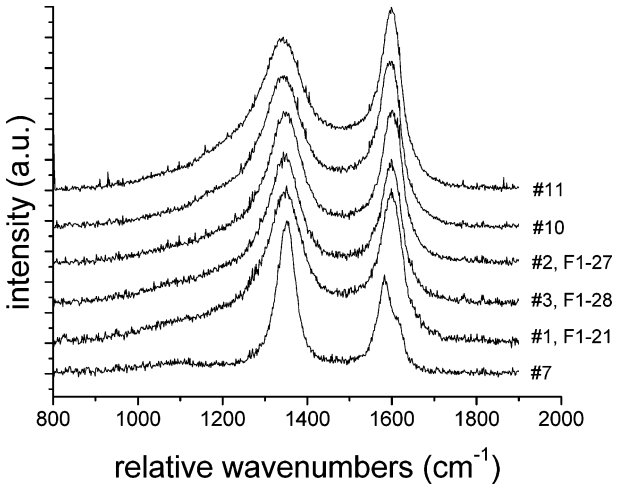

Figure 13. Raman spectra of batches #1−3, #7, #10, and #11.

dispersion effect of catalyst particles described for a transition metal/multiwall nanotube mixture[43] holds for CNFs too.

The formation of nanotube-type fiber fuzz (Figure 14d) may be related to pyrolytic carbon surface layers which stem from polymerization of C_2H_2 molecules during fiber processing. Their growth may be enhanced via redistribution/enrichment of fine-grained catalyst particles as described above.

A TEM investigation of CNF batches exposed to high-temperature activation followed by an uptake of hydrogen virtually reveals the same microstructural pattern as previously discussed solely for the effect of activation. This is displayed for batch #3 (Table 2) in Figure 16a−c emphasizing that during the activation stage already the fibers are prone to a continuous loss of structural integrity.

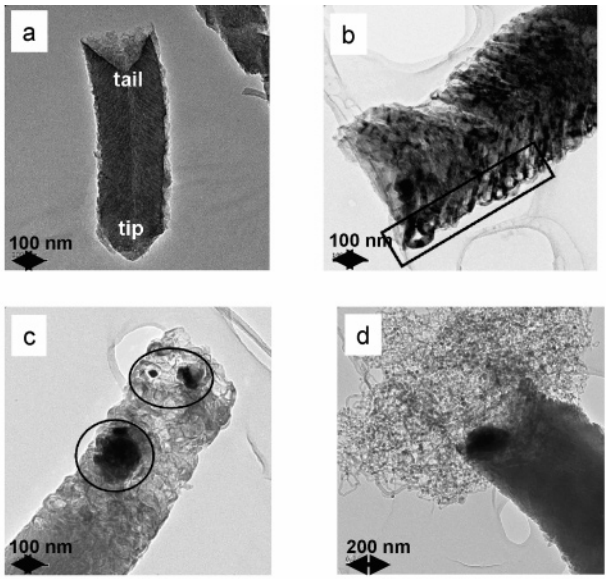

Figure 14. Microstructural changes of CNF batch #2 (specimen F1-27 from Catalytic Materials Inc.) upon activation in argon atmosphere (TEM bright field images): (a) pristine fiber morphology defining tip vs tail sections, (b) loss of herringbone architecture (initial stage, tail section) and formation of graphitic carbon loops at fiber surface (see boxed area), (c) loss of herringbone architecture (mature stage, tip section) associated with notable enrichment of catalyst particles (encircled areas), and (d) formation of secondary extremely fine-grained nanotube-type fuzz at fiber tail section.

In addition to the procedure describe earlier, we also tested some slightly modified activation procedures. For instance, in some cases a custom-built transfer system was used to transfer the fibers from the activation system to the hydrogen storage vessel under anaerobic conditions.

4.2. Hydrogen Storage. Investigation of the different nanofiber batches by thermodesorption (TDS) yields similar results for all fibers investigated; Figure 17 shows a typical spectrum. The key fragments hydrogen (02), water (18), and carbon monoxide (28) as monitored by a mass spectrometer as a function of time are presented; additional mass fragments necessary for the correct assignment are suppressed for a better clarity of the plot. No significant desorption of hydrogen- or carbon-containing fragments at moderate temperatures is detected.

A hydrogen release starting at 600 °C is remarkable. This high-temperature hydrogen is found for all fibers. It varies from 0.1 to 1 wt % as found after semiquantitative analysis with a calibration volume and confirmed by elementary analysis. In their publications,[3,38] Rodriguez and Baker claimed this high-temperature peak to be an indicator for the presence of a hydrogen storing material. They interpret this effect as a small part of the stored hydrogen, which can be released only at high

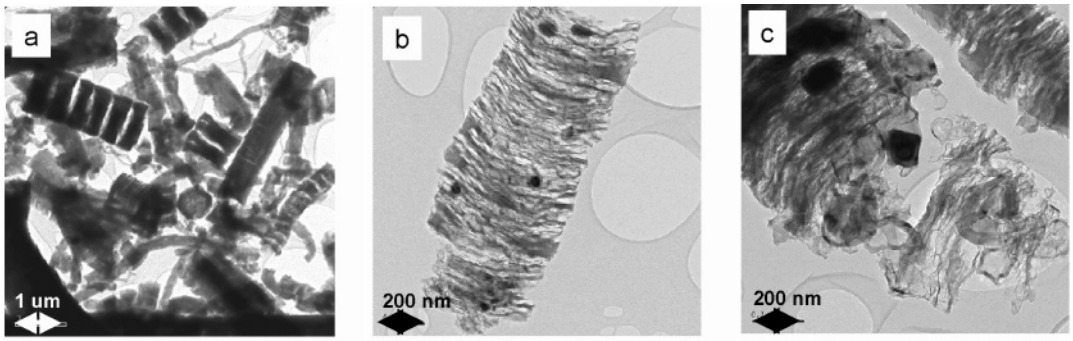

Figure 15. Microstructural changes of CNF batch #8 (Table 2) upon activation in argon atmosphere (TEM bright field images): (a) segmented fiber architecture in the as-received condition, (b and c) loss of structural integrity of the fiber and enrichment of catalyst particles.

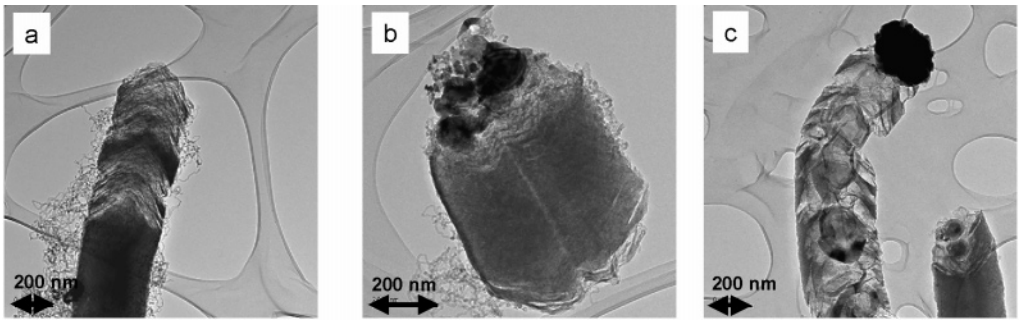

Figure 16. Microstructural changes of CNF batch #3 (specimen F1−28, Catalytic Materials Inc.) upon both activation in argon atmosphere and hydrogen uptake (TEM bright field images): (a and b) various stages of disintegration of graphic layers at CNF tip and tail sections associated with enrichment of catalyst particles. Note the formation of very fine-grained tubular fiber fuzz at the fiber surface adjacent to disintegrated areas, (c) complete loss of CNF herringbone architecture of graphene sheets.

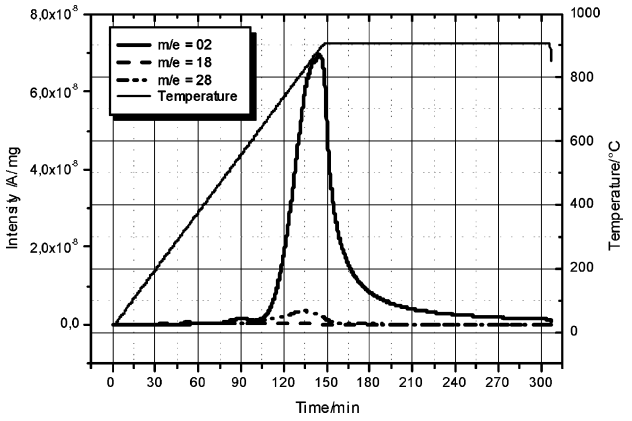

Figure 17. Thermodesorption spectrum of sample #4.

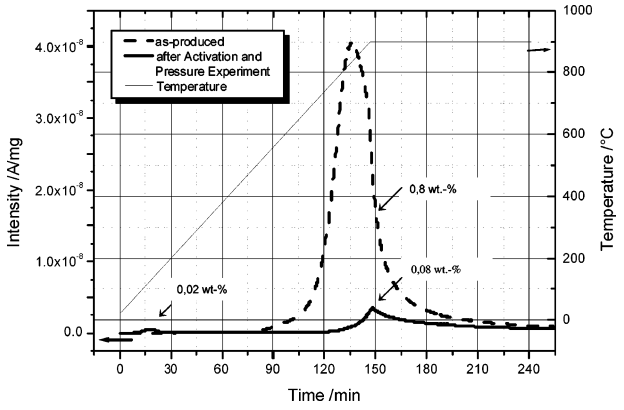

Figure 18. Thermodesorption of hydrogen from sample #3, both for pristine fiber (dashed line) and for fibers which have been exposed to 130 bar hydrogen (solid line).

temperatures because it is chemisorbed at the fibers. If this is the case, the exposure of the fibers to hydrogen should reproduce the peak. However, after the samples were exposed to hydrogen at 1 bar, only a very small peak of desorbing hydrogen around 120 °C, corresponding to 0.02 wt %, is found (Figure 18). The peak at 850 °C does not appear again; therefore it is unlikely that it is related with a reversible adsorption−desorption property of the material.

What remains unclear is the origin of the hydrogen observed in the TDS experiment. Through the use of TDS, it is impossible to distinguish between hydrogen located inside or outside of the carbon nanofiber. Since at the applied temperatures the cracking of covalent C−H-bonds is expected, the hydrogen may cause hydrogen-saturated edges of the graphene sheets. Further studies are needed to clarify these facts.

Table 4 summarizes the results of the volumetric and gravimetric hydrogen storage measurements of the samples under investigation. The major part of these measurements has been done with the volumetric absorption apparatus and the gravimetric apparatus. If available, we show also the results of the volumetric desorption measurements. As in the desorption experiments, all samples gave values below the limit of detection; this gives an upper limit for the released hydrogen. In addition to the measurements for pristine samples, Table 4 also contains the results for activated samples. Besides the activation procedure described above (labeled "925 °C Ar"), we also show measurements for samples, which are only heated at 190 °C under argon flow (labeled "190 °C Ar") and helium flow (labeled "190 °C He"). In general, the measured hydrogen uptake is low for all samples. Within the experimental error (in the order of 0.1 wt % for most samples), only samples #1 and #2 show a significant hydrogen uptake up to 0.4 wt % but far below values of 2−4%.

Complementary data derived via thermal desorption measurements (Table 5) after exposing the samples to hydrogen at a pressure above 100 bar also show no uptake within the range of the experimental error.

TABLE 4: Hydrogen Storage Capacity of the Nanofiber Samples As Measured with the Volumetric Adsorption Apparatus in wt %

sample #1	50 bar[a]	95 bar	140 bar
pristine	0.14	0.33	0.39
190 °C Ar	0.12	0.19	0.24
925 °C Ar	0.11 (0.19)	0.24 (0.26)	0.22 (0.36)
sample #2	50 bar[a]	95 bar	140 bar
pristine	0.10	0.22	0.29
190 °C Ar	0.05	0.06	0.25
925 °C Ar	0.11 (<0.10)	0.15 (<0.10)	0.14 (<0.10)
sample #3	50 bar[a]	95 bar	140 bar
pristine	0.04 (<0.10)	0.03 (<0.10)	−0.09 (<0.10)
190 °C Ar	0.07	0.05	−0.05
925 °C Ar	−0.08 (<0.10)	−0.12 (<0.10)	−0.20 (<0.10)
sample #4	50 bar[a]	95 bar	140 bar
190 °C He	0.03	0.08	0.09
sample #5	50 bar[a]	95 bar	140 bar
pristine	0.00	0.00	−0.07
190 °C Ar	−0.03	−0.03	−0.04
sample #6	50 bar[a]	95 bar	140 bar
190 °C He	0.03	0.06	0.20
sample #7	50 bar[a]	95 bar	140 bar
pristine	0.13		
250 °C	−0.14		
sample #8	50 bar[a]	95 bar	140 bar
925 °C Ar	0.03	0.04	0.05
sample #9	50 bar[a]	95 bar	140 bar
pristine	0.13	0.09	0.02

[a] If available, the gravimetric value is given in parentheses. The experimental error of all measurements is approximately ±0.1 wt %.

TABLE 5: Hydrogen Storage Capacities Determined by Desorption Measurements

sample	activation	pressure	storage capacity[a]
#1	150 °C.	130 bar	−0.2 wt %
	vacuum 1000 °C.Ar/H_2	120 bar	0.8 wt %
#2	150 °C.	120 bar	−1.0 wt %
	vacuum 900 °C.	100 bar	0.2 wt %
	vacuum 1000 °C. Ar/H_2	120 bar	−1.0 wt %
#3	150 °C.	100 bar	0.5 wt %
	vacuum 925 °C. Ar	100 bar	−0.3 wt %
#4	150 °C. vacuum	130 bar	0.5 wt %
			−0.3 wt %
#6	150 °C. vacuum	130 bar	0.7 wt %
			0.4 wt %
#7	150 °C.	130 bar	0.1 wt %
	vacuum 700°C Ar/O_2	130 bar	0.1 wt %
#8	150 °C.	100 bar	−0.1 wt %
	vacuum, 150 °C.	120 bar	−1.0 wt %
	vacuum 925 °C. Ar	100 bar	−0.2 wt %
#9	1000 °C. Ar/H_2	120 bar	−0.8 wt %

[a] Note: The standard deviation of this procedure as derived from dry runs was about 0.8 wt %.

In addition, no increase of the hydrogen uptake due to activation procedures could be detected. On the contrary, the two pristine samples #1 and #2, which show a slight storage capacity, lose this property by the activation. This is in accordance with the TEM analysis of the fibers, which shows a strong structural change due to the high-temperature treatment.

In particular, we were not able to confirm the hydrogen storage values of 1.5 and 4.2 wt % provided by Baker and Rodriguez for their sample #5 in the pristine state and after activation, respectively.

5. Conclusion

Within the framework of the study presented, we investigated carbon nanofibers provided by the Rodriguez and Baker group as well as nanofibers synthesized in our labs following the procedures published by different research groups working in this field. The batches comprise different structural and morphological characteristics. The fibers were analyzed with respect to their hydrogen uptake at room temperature in the pressure range from 0 to 140 bar using gravimetric and volumetric techniques. In some cases, additional activation procedures were applied to the pristine fibers prior to the hydrogen storage experiments. Within the experimental error of 0.1 wt %, we obtained good agreement between the two high-precision experimental techniques applied for quantification of hydrogen uptake. However, no significant hydrogen uptake could be detected for any of the CNF specimens investigated. With a maximum uptake of 0.4 wt %, all experimental results can be adequately explained by pure physical adsorption on the CNF surface; no evidence for any other storage mechanism has been found. We therefore were unable to confirm the data published by other groups reporting hydrogen storage capacities for CNFs above 3 wt %.

Acknowledgment. The financial support from the German Federal Ministry of Economics and Labor (BMWi) through Grant 0327304 is kindly acknowledged. We would like to thank R.T.K. Baker, and N.M. Rodriguez for providing us with different carbon nanofiber material and the information about the adequate fiber pretreatment procedure. The authors would also like to acknowledge Prof. W. Kiefer and co-workers at Physical Chemistry, Würzburg University, for providing the Raman characterization.

References and Notes

(1) *New Sci.* **1996**, *2061*, 20.
(2) Chambers, A.; Park, C.; Baker, T. K.; Rodriguez, N. M. *J. Phys. Chem. B* **1998**, *102*, 4253.
(3) Park, C.; Anderson, P. E.; Chambers, A.; Tan, C. D.; Hidalgo, R.; Rodriguez, N. M. *J. Phys. Chem. B* **1999**, *103*, 10572.
(4) Boehm, H. P. *Carbon* **1973**, *11*, 583.
(5) Baker, R. T. K.; Barber, M. A.; Harris, P. S.; Feates, F. S.; Waite, R. J. *J. Catal.* **1972**, *26*, 51.
(6) Yang, R. T.; Chen, J. P. *J. Catal.* **1989**, *115*, 52.
(7) Baker, R. T. K. *Carbon* **1989**, *27*, 315.
(8) Rodriguez, N. M. *J. Mater. Res.* **1993**, *8*, 3233.
(9) Krishnankutty, N.; Park, C.; Rodriguez, N. M.; Baker, R. T. K. *Catal. Today* **1997**, *37*, 295.
(10) Rodriguez, N. M.; Chambers, A.; Baker, R. T. K. *Langmuir* **1995**, *11*, 3862.
(11) Cheng, H.-M.; Yang, Q.-H.; Liu, C. *Carbon* **2001**, *39*, 1447.
(12) Baker, R. T. K.; Rodriguez, N. M. Graphite nanofiber catalyst systems for use in fuel cell electrodes. U.S. Patent 6,485,858, 2002.
(13) Endo, M.; Kim, C.; Nishimura, K.; Fujino, T.; Miyashita, K. *Carbon* **2000**, *38* 183.
(14) Rodriguez, N. M.; Kim, M.-S.; Baker, R. T. K. *J. Phys. Chem.* **1994**, *98*, 13108.
(15) Chen, P.; Wu, X.; Lin, J.; Tan, K. L. *Science* **1999**, *285*, 91.
(16) Yang, R. T. *Carbon* **2000**, *38* 623.
(17) Fan, Y.; Liao, B.; Liu, M.; Yei, Y.; Lu, M.; Cheng, H. *Carbon* **1999**, *37*, 1649.
(18) Cheng, F.; et al. *Z. Metallkd.* **2000** *91*, 306.
(19) Gupta, B. K.; Srivastava, O. N. *Int. J. Hydrogen Energy* **2000**, *25*, 825.
(20) Gupta, B. K.; Srivastava, O. N. *Int. J. Hydrogen Energy* **2001**, *26*, 857.
(21) Browning, D. J.; Gerrard, M. L.; Lakeman, J. B.; Mellor, I. M.; Mortimer, R. J.; Turpin, M. C. *Nano Lett.* **2002**, *3*, 201.
(22) Ströbel, R.; Jörissen, L.; Schliermann, T.; Trapp, V.; Schütz, W.; Bohmhammel, K.; Wolf, G.; Garche, J. *J. Power Sources* **1999**, *84*, 221.
(23) Ahn, C. C.; Ye, Y.; Ratnakumar, B. V.; Witham, C.; Bowman, R. C.; Fultz, B. *Appl. Phys. Lett.* **1998**, *73*, 3378.

(24) Poirier, E.; Chahine, R.; Bose, T. K. *Int. J. Hydrogen Energy* **2001**, *26*, 831.
(25) Hirscher, M.; et al. *J. Alloys Compd.* **2002**, *330*, 654.
(26) Tibbetts, G. G.; Meisner, G. P.; Olk, C. H. *Carbon* **2001**, *39*, 2291.
(27) Baker, R. T. K.; Rodriguez, N. M. Private communication, 2002.
(28) Hirscher, M.; Becher, M. *J. Nanosci. Nanotechnol.* **2003**, *3*, 3.
(29) Ritschel, M.; Uhlemann, M.; Gutfleisch, O.; Leonhardt, A.; Graff, A.; Täschner, Ch.; Fink, J. *Appl. Phys. Lett.* **2002**, *80*, 2985.
(30) Rodriguez, N. M.; Baker, T. K. Private communication, 2002.
(31) Rodriguez, N. M.; Kim, M.; Baker, R. T. K. *J. Catal.* **1993**, *140*, 16.
(32) Gregg, S. J.; Sing, K. S. Adsorption, Surface Area and Porosity; Academic Press: London, 1982.
(33) Kinoshita, K. Carbon: Electrochemical and Physicochemical Properties; John Wiley & Sons: New York, 1988.
(34) Ferrari, A. C.; Robertson, J. *Phys. Rev. B* **2000**, *61*, 14095.
(35) Rzepka, M.; Lamp, P.; de la Casa-Lillo, M. A. *J. Phys. Chem. B* **1998**, *102*, 10894.
(36) Hycob GmbH, Moers. www.hycob.de.
(37) Chen, X. H.; Deng, F. M.; Lu, X. N.; Wu, G. T.; Wang, M.; Yang, H. S.; Zhang, X. B. *J. Cryst. Growth* **2001**, *222*, 163.
(38) Rodriguez, N. M.; Baker, R. T. K. International Patent WO00/76625 A1, 2000.
(39) Fricke; et al. Innovative Energiespeicher auf der Basis von Kohlenstoffnanostrukturen, Abschlussbericht, FKZ 0327304D; Report E21-0203-2, 2003.
(40) Rodriguez, N. M.; Baker, T. K. Private communication
(41) Endo, M.; Kim, Y. A.; Hayashi, T.; Yanagisawa, T.; Muramatsu, H.; Ezaka, M.; Terrones, H.; Terrones, M.; Dresselhaus, M. S. *Carbon* **2003**, *41*, 1941.
(42) Zheng, G. B.; Sano, H.; Uchiyama, Y. *Carbon* **2003**, *41*, COI-856.
(43) Zhong, Z.; Liu, B.; Sun, L.; Ding, J.; Lin, J.; Tan, K. I. *Chem. Phys. Lett*. **2002**, *362*, 135.